ANALYSIS OF A LAMINATED COMPOSITE WIND TURBINE BLADE CHARACTERISTICS THROUGH MATHEMATICAL APPROACH

YOUNG-DO CHOI[1], JAEGWI GO[2†], AND SEOKCHAN KIM[3]

[1]DEPARTMENT OF MECHANICAL ENGINEERING, MOKPO NATIONAL UNIVERSITY, SOUTH KOREA
Email address: ydchoi@mokpo.ac.kr

[2]DEPARTMENT OF MATHEMATICS, CHANGWON NATIONAL UNIVERSITY, SOUTH KOREA
Email address: jggo@changwon.ac.kr

[3]DEPARTMENT OF MATHEMATICS, CHANGWON NATIONAL UNIVERSITY, SOUTH KOREA
Email address: sckim@changwon.ac.kr

ABSTRACT. A 1kW-class horizontal axis wind turbine (HAWT) rotor blade is taken into account to investigate elastic characteristics in 2-D. The elastic blade field is composed of symmetric cross-ply laminated composite material. Blade element momentum theory is applied to obtain the boundary conditions pressuring the blade, and the plane stress elasticity problem is formulated in terms of two displacement parameters with mixed boundary conditions. For the elastic characteristics a fair of differential equations are derived based on the elastic theory. The domain is divided by triangular and rectangular elements due to the complexity of the blade configuration, and a finite element method is developed for the governing equations to search approximate solutions. The results describe that the elastic behavior is deeply influenced by the layered angle of the middle laminate and the stability of the blade can be improved by controlling the layered angle of laminates, which can be evaluated by the mathematical approach.

1. INTRODUCTION

By taking advantage of low operation and maintenance cost, and fast installation wind turbine is highlighted as an electricity production generator. Since free and renewable energies are employed to produce electricity, wind turbine is a representative generator of pollution free electricity. But, due to the critical demerit, the temporary nature of wind flow, reliable and efficient blade design has been a matter of primary concern in order to obtain the maximum energy from wind during the limited flowing period. Nowadays, composite materials (CMs) are used in manufacturing blades to satisfy complex design constraints such as lower weight

and proper stiffness, while providing good resistance to the static and fatigue loading. In designing wind turbine blades important factors to be considered for lifetime extension are: (i) Long and flexible structures; (ii) Vibrations in its resonant mode; (iii) Randomness in the load spectra due to the nature of the wind; (iv) Continuous operation under different conditions; (v) Low maintenance during lifetime [1].

In structural elements CMs display better performance owing to the excellent strength and stiffness ratio to weight ratios, structural tailoring capability and tolerance to damage, and have been used actively in engineering applications such as aerospace, marine, and automotive. The excellent strength and stiffness ratio to weight ratios plays an important role, especially, in the application of wind turbines. However, the process of ply drop-off to form CMs yields low shear modulus, causing weaker compression strength in comparison with tensile. Various structural elements, in general, are subjecting both loads and constraint at the same time during the service and the materials composed of the elementals suffer from large deflections and stresses in the presence of inherent scatter in the material properties under random loadings. The capability to predict failure mechanisms like the maximum load and the elastic characteristics of laminated CMs, thus, is a crucial part for reliable performance in applications.

Lifetime prediction and analysis of failure mechanisms for wind turbine composite blades have been studied by many authors for reliability assurance. Mahmood *et. al.* [2] considered a HAWT composite blade and static analysis is performed to extract the critical zone where fatigue failure begins using a full 3-D finite element method. The responses of applying a torsional loading to a laminated composite blade made of thermosetting epoxy matrix reinforced by glass fibers were investigated by Tseng and Kuo [3].The composite blade of a small 1 kW wind generator system showed that the weakest location of the blade is at the interface of the aluminum shaft and glass-fiber/epoxy lay-ups in the composite blade root. Overgaard *et. al.* [4] suggested a modeling strategy, sub-modeling approach, for the structural analysis of large 3-dimensional laminated composite structures undergoing geometric and material induced instability. The strategy is for tracking multiple crack formations and the propagation of multiple delamination fronts. The fatigue behavior of the material and structural properties were highlighted on wind turbine rotor blades made of composite materials by Kensche [5], considering the influence of fiber content and architecture and environmental effects. Ghasemnejad *et. al.* [6] presented the inter-laminar damage due to low velocity impacts on hybrid composite materials typical of those used in wind turbine blade structures, investigating the post-buckling behavior of multi-delaminated composite beam. The effectiveness of a materials and design selection methodology for a small low air-speed composite wind turbine blade is studied by Aceves *et. al.* [7] – [8]. Lindaard and Lund [9] presented an approach to nonlinear buckling fiber angle optimization of laminated composite shell structures, explaining the geometrically nonlinear behavior of the structure by utilizing response analysis up until the critical point. The interactions of composite box beams, showing various failure modes due to competing failure mechanism, have been investigated using finite element method by Chen *et. al.* [10] They analyzed failure mechanisms occurring in the composite box, by considering three types of structural nonlinearities which is caused from geometry, materials, and contact. Lee [11] presented a damping mechanism model based on fluid inertia damping caused by a delayed

response of flow development. They concluded that the fluid inertia damping is a dominant factor for a larger composite wind turbine blade in faster oscillatory motion. Furthermore, Euler-Bernoulli beam theory has been adopted for the analysis of composite turbine blades and extended to a generalized Timoshenko beam theory. The applications of a generalized Timoshenko beam theory for composite wind turbine blades are performed with cross-sectional analysis. Giavotto *et. al.* [12] proposed an improved accuracy method saint venant beam theory (SVBT), which was stereotyped as the beam cross section analysis software (BECAS) by Blasques *et. al.* [13]. Hodges *et. al.* [14] induced a developed method variational asymptotic beams section analysis (VABS) and VABS is widely used for the analysis of composite wind turbine blades [15] – [17].

Even though many authors have been tried to analyze the failure mechanisms and fatigue behavior, as referenced above, the generalization is still remained as a one of the biggest challenge in wind turbine aerodynamics. Therefore, in the present study, in order to reduce high cost to design an effective rotor blade and trial and error period, mathematical approach to the elastic characteristics of the blade is required, and a newly developed mathematical modeling method is suggested. A 1kW-class horizontal axis wind turbine (HAWT) rotor blade is considered to investigate the elastic characteristics of composite blade. Blade element momentum theory is applied to obtain the boundary conditions pressuring blade and continuum mechanic theory is developed for elastic behavior.

2. MATHEMATICAL MODELING

2.1. **Blade element momentum theory.** Blade element momentum theory is developed under the assumptions: (i) No aerodynamic interactions appear between different blade elements, (ii) The forces on the blade elements are solely determined by the lift and drag coefficients, (iii) the flow is frictionless, which gives the axial force F_x

$$dF_x = \frac{1}{2}U_\infty^2[4a(1-a)]2\pi r dr,$$

the tangential force F_θ

$$dF_\theta = 4\acute{a}(1-a)\pi\rho U_\infty\Omega r^2 dr,$$

and the tangential force T [18]

$$dT = 4\acute{a}(1-a)\pi\rho U_\infty\Omega r^3 dr.$$

U represents the flow velocity, ρ the air density, ω the wake rotational speed, and Ω the blade rotational speed, and the axial induction factor and angular induction factor are defined by
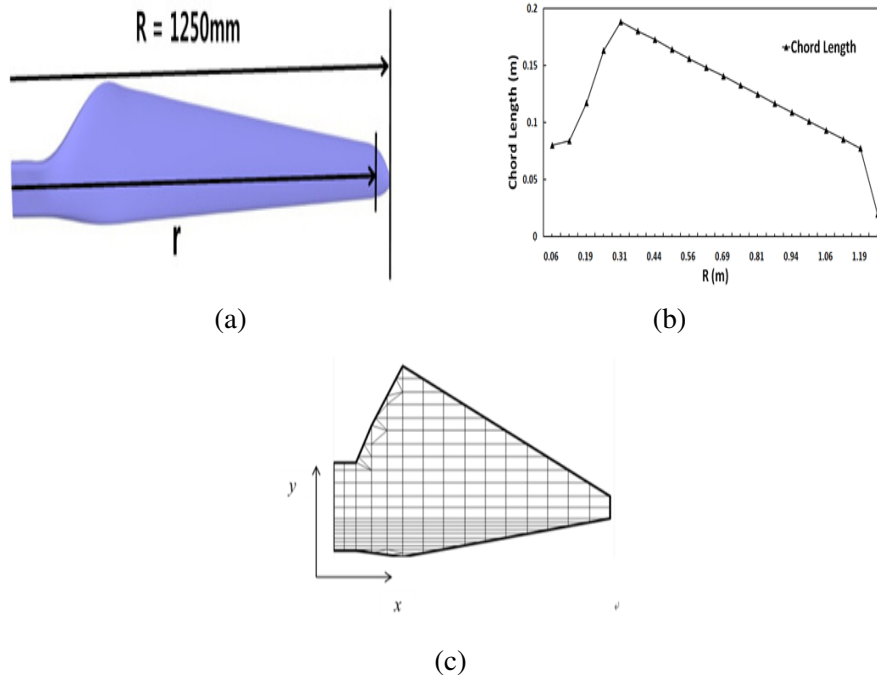
$$a = \frac{U_\infty - U_d}{U_\infty}$$

and

FIGURE 1. Schematic view of 1kW-class HAWT rotor blade model : (a) longitudinal length, (b) chord length, (c) Discretized mesh of the blade model for numerical analysis.

$$á = \frac{\omega}{2\Omega},$$

respectively. The symbol ∞ refers to conditions far upstream and d refers to conditions at the disc. In addition, under the assumption that the forces on a blade element can be calculated by means of two dimensional aero foil characteristics using an angle of attack determined from the incident resultant velocity in the cross-sectional plane of the element, the relative flow angle ϕ onto blades is defined by

$$\sin \phi = \frac{U_\infty(1-a)}{W},$$

where W is the relative velocity. The relation between the angle of attack α and the pitch angle β is then given by

$$\alpha = \phi - \beta.$$

2.2. **Composite laminated theory.** By the considering of a symmetric cross-ply laminated composite field the average stress-strain relations in principal material coordinates in plane (see Fig. 1(b)) for a lamina can be formulated as

$$
\begin{bmatrix} \sigma_x \\ \sigma_y \\ \tau_{xy} \end{bmatrix} = \frac{1}{h} \begin{bmatrix} A_{11} & A_{12} & 0 \\ A_{12} & A_{22} & 0 \\ 0 & 0 & A_{66} \end{bmatrix} \begin{bmatrix} \varepsilon_x \\ \varepsilon_y \\ \gamma_{xy} \end{bmatrix}
$$

The h is to the total thickness of the laminate. The element of stiffness matrix $[A]$ for a symmetric laminate with n-multiple orthotropic layers are

$$
A_{ij} = \sum_{k=1}^{n} [\bar{Q}_{ij}]_k (h_k - h_{k-1}),
$$

where

$$
[\bar{Q}_{11}]_k = [Q_{11}]_k \cos^4 \theta_k + [Q_{22}]_k \sin^4 \theta_k + (2[Q_{12}]_k + 4[Q_{66}]_k) \cos^2 \theta_k \sin^2 \theta_k
$$
$$
[\bar{Q}_{12}]_k = ([Q_{11}]_k + [Q_{22}]_k - 4[Q_{66}]_k) \cos^2 \theta_k \sin^2 \theta_k + [Q_{12}]_k (\cos^4 \theta_k + \sin^4 \theta_k)
$$
$$
[\bar{Q}_{22}]_k = [Q_{11}]_k \sin^4 \theta_k + [Q_{22}]_k \cos^4 \theta_k + (2[Q_{12}]_k + 4[Q_{66}]_k) \cos^2 \theta_k \sin^2 \theta_k
$$
$$
[\bar{Q}_{66}]_k = ([Q_{11}]_k + [Q_{22}]_k - 2[Q_{12}]_k - 2[Q_{66}]_k) \cos^2 \theta_k \sin^2 \theta_k + [Q_{66}]_k (\cos^4 \theta_k + \sin^4 \theta_k)
$$

$$
[Q_{11}]_k = \frac{E_1^k}{1 - \nu_{12}^k \nu_{21}^k} \qquad [Q_{21}]_k = \frac{\nu_{21}^k E_1^k}{1 - \nu_{12}^k \nu_{21}^k} \qquad [Q_{22}]_k = \frac{E_2^k}{1 - \nu_{12}^k \nu_{21}^k}
$$
$$
[Q_{16}]_k = 0 \qquad\qquad [Q_{26}]_k = 0 \qquad\qquad [Q_{66}]_k = G_{12}^k.
$$

Here $(h_k - h_{k-1})$ is the thickness of the $k - th$ ply of the laminate, θ_k is the angle between the x-axis and the fiber direction of a laminate in the laminate, E_1^k and E_2^k are the Young's modulus of the $k - th$ ply in the longitudinal and transverse directions, respectively, ν_1^k and ν_2^k are the major and minor Poison's ratio of the $k - th$ ply, respectively, and G_{12}^k is the in-plain shear modulus of a laminate in the laminate [19]. The basic stress can be expressed in terms of displacements as

$$
\sigma_x = \frac{1}{h} [A_{11} \frac{\partial u_x}{\partial x} + A_{12} \frac{\partial u_y}{\partial y}]
$$
$$
\sigma_y = \frac{1}{h} [A_{12} \frac{\partial u_x}{\partial x} + A_{22} \frac{\partial u_y}{\partial y}]
$$
$$
\tau_{xy} = \frac{1}{h} [A_{66} (\frac{\partial u_x}{\partial y} + \frac{\partial u_y}{\partial x})]. \tag{2.1}
$$

The u_x and u_y refer to the displacement components in the x- and y- directions, respectively. The equation of equilibrium for the plane elasticity problems are given by

$$\frac{\partial \sigma_x}{\partial x} + \frac{\partial \tau_{xy}}{\partial y} - \rho\Omega^2 x = 0,$$

$$\frac{\partial \sigma_y}{\partial y} + \frac{\partial \tau_{xy}}{\partial x} - \rho\Omega^2 y = 0. \tag{2.2}$$

where Ω is the blade rotational speed. The combination of equations 2.1 and 2.2 yields

$$\frac{\partial}{\partial x}[A_{11}\frac{\partial u_x}{\partial x} + A_{12}\frac{\partial u_y}{\partial y}] + \frac{\partial}{\partial y}[A_{66}(\frac{\partial u_x}{\partial y} + \frac{\partial u_y}{\partial x})] - h\rho\Omega^2 x = 0, \tag{2.3a}$$

$$\frac{\partial}{\partial x}[A_{66}(\frac{\partial u_x}{\partial y} + \frac{\partial u_y}{\partial x})] + \frac{\partial}{\partial y}[A_{12}\frac{\partial u_x}{\partial x} + A_{22}\frac{\partial u_y}{\partial y}] - h\rho\Omega^2 y = 0. \tag{2.3b}$$

The boundary conditions for the present wind blade are obtained through the process in Sect. 2.1 and used for numerical approximation.

2.3. Finite element formulation.
Since the governing equation 2.3 is too involved to solve analytically, the partial differential equations convert into a linear system based on a finite element method consisting of triangular and rectangular elements. Now, the variational approach for the equations 2.3 is developed based on a finite element method. Multiplication equation 2.3b by a trial function w_1 and equation 2.3b by w_2, and integration over the domain yields the followings:

$$\int_\Lambda [\frac{\partial w_1}{\partial x}(A_{11}\frac{\partial u_x}{\partial x} + A_{12}\frac{\partial u_y}{\partial y}) + \frac{\partial w_1}{\partial y}(A_{66}\frac{\partial u_y}{\partial x} + A_{66}\frac{\partial u_x}{\partial y})]dA$$

$$= -\oint_\Gamma w_1 t_x ds + \int_\Lambda w_1 h\rho\Omega^2 x dA,$$

$$\int_\Lambda [\frac{\partial w_2}{\partial x}(A_{66}\frac{\partial u_y}{\partial x} + A_{66}\frac{\partial u_x}{\partial y}) + \frac{\partial w_2}{\partial y}(A_{12}\frac{\partial u_x}{\partial x} + A_{22}\frac{\partial u_y}{\partial y})]dA$$

$$= -\oint_\Gamma w_2 t_y ds + \int_\Lambda w_2 h\rho\Omega^2 y dA,$$

where

$$t_x = n_x(A_{11}\frac{\partial u_x}{\partial x} + A_{12}\frac{\partial u_y}{\partial y}) + n_y(A_{66}\frac{\partial u_y}{\partial x} + A_{66}\frac{\partial u_x}{\partial y}),$$

$$t_y = n_x(A_{66}\frac{\partial u_y}{\partial x} + A_{66}\frac{\partial u_x}{\partial y}) + n_y(A_{12}\frac{\partial u_x}{\partial x} + A_{22}\frac{\partial u_y}{\partial y})$$

are the tractions on Γ. The domain Λ is divided into subdomains, Λ^e, $e = 1, 2, ..., N$, and the variational form over the each element Λ^e is

$$\int_{\Lambda^e}[\frac{\partial w_1}{\partial x}(A_{11}\frac{\partial u_x}{\partial x} + A_{12}\frac{\partial u_y}{\partial y}) + \frac{\partial w_1}{\partial y}(A_{66}\frac{\partial u_y}{\partial x} + A_{66}\frac{\partial u_x}{\partial y})]dA$$
$$= -\oint_{\Gamma^e} w_1 t_x ds + \int_{\Lambda^e} w_1 h\rho\Omega^2 x dA,$$

$$\int_{\Lambda^e}[\frac{\partial w_2}{\partial x}(A_{66}\frac{\partial u_y}{\partial x} + A_{66}\frac{\partial u_x}{\partial y}) + \frac{\partial w_2}{\partial y}(A_{12}\frac{\partial u_x}{\partial x} + A_{22}\frac{\partial u_y}{\partial y})]dA$$
$$= -\oint_{\Gamma^e} w_2 t_y ds + \int_{\Lambda^e} w_2 h\rho\Omega^2 y dA. \tag{2.4}$$

Let us define

$$B^{11}(w_1, u_x) = \int_{\Lambda^e}[\frac{\partial w_1}{\partial x} A_{11}\frac{\partial u_x}{\partial x} + \frac{\partial w_1}{\partial y} A_{66}\frac{\partial u_x}{\partial y}]dA$$

$$B^{12}(w_1, u_y) = \int_{\Lambda^e}[\frac{\partial w_1}{\partial x} A_{12}\frac{\partial u_y}{\partial y} + \frac{\partial w_1}{\partial y} A_{66}\frac{\partial u_y}{\partial x}]dA$$

$$B^{21}(w_2, u_x) = \int_{\Lambda^e}[\frac{\partial w_2}{\partial x} A_{66}\frac{\partial u_x}{\partial y} + \frac{\partial w_2}{\partial y} A_{12}\frac{\partial u_x}{\partial x}]dA$$

$$B^{22}(w_2, u_y) = \int_{\Lambda^e}[\frac{\partial w_2}{\partial x} A_{66}\frac{\partial u_y}{\partial x} + \frac{\partial w_2}{\partial y} A_{22}\frac{\partial u_y}{\partial y}]dA$$

$$l^1(w_1) = -\oint_{\Gamma^e} w_1 t_x ds + \int_{\Lambda^e} w_1 h\rho\Omega^2 x dA$$

$$l^2(w_2) = -\oint_{\Gamma^e} w_2 t_y ds + \int_{\Lambda^e} w_2 h\rho\Omega^2 y dA.$$

then equations 2.4 are of the form

$$B^{11}(w_1, u_x) + B^{12}(w_1, u_y) = l^1(w_1)$$
$$B^{21}(w_2, u_x) + B^{22}(w_2, u_y) = l^2(w_2). \tag{2.5}$$

Suppose that on an element e

$$u_x \approx \sum_{j=1}^{n} u_j^{(e)}\phi_j^{(e)}, \quad u_y \approx \sum_{j=1}^{n} v_j^{(e)}\phi_j^{(e)}.$$

The $u_j^{(e)}$, $v_j^{(e)}$ are the nodal values of the primary variables. By employing the Ritz method the variational form 2.5 can be written by

$$\sum_{j=1}^{n} B^{11}(\phi_i^{(e)}, \phi_j^{(e)})u_j^{(e)} + \sum_{j=1}^{n} B^{12}(\phi_i^{(e)}, \phi_j^{(e)})v_j^{(e)} = l^1(\phi_i^{(e)})$$

$$\sum_{j=1}^{n} B^{21}(\phi_i^{(e)}, \phi_j^{(e)})u_j^{(e)} + \sum_{j=1}^{n} B^{22}(\phi_i^{(e)}, \phi_j^{(e)})v_j^{(e)} = l^2(\phi_i^{(e)}).$$

or

$$[K^{11(e)}]\{u^{(e)}\} + [K^{12(e)}]\{v^{(e)}\} = \{F^{1(e)}\}$$
$$[K^{21(e)}]\{u^{(e)}\} + [K^{22(e)}]\{v^{(e)}\} = \{F^{2(e)}\}. \tag{2.6}$$

The matrix elements represent, respectively,

$$K_{ij}^{11(e)} = \int_{\Lambda^e}[A_{11}\frac{\partial\phi_i^{(e)}}{\partial x}\frac{\partial\phi_j^{(e)}}{\partial x} + A_{66}\frac{\partial\phi_i^{(e)}}{\partial y}\frac{\partial\phi_j^{(e)}}{\partial y}]dA$$

$$K_{ij}^{12(e)} = K_{ij}^{21(e)} = \int_{\Lambda^e}[A_{12}\frac{\partial\phi_i^{(e)}}{\partial x}\frac{\partial\phi_j^{(e)}}{\partial y} + A_{66}\frac{\partial\phi_i^{(e)}}{\partial y}\frac{\partial\phi_j^{(e)}}{\partial x}]dA$$

$$K_{ij}^{22(e)} = \int_{\Lambda^e}[A_{66}\frac{\partial\phi_i^{(e)}}{\partial x}\frac{\partial\phi_j^{(e)}}{\partial x} + A_{22}\frac{\partial\phi_i^{(e)}}{\partial y}\frac{\partial\phi_j^{(e)}}{\partial y}]dA$$

$$F^{1(e)} = -\oint_{\Gamma^e}\phi_i^{(e)}t_x ds + \int_{\Lambda^e}\phi_i^{(e)}h\rho\Omega^2 x dA$$

$$F^{2(e)} = -\oint_{\Gamma^e}\phi_i^{(e)}t_y ds + \int_{\Lambda^e}\phi_i^{(e)}h\rho\Omega^2 y dA.$$

Equations 2.6 can be expressed with

$$\begin{bmatrix} K^{11(e)} & K^{12(e)} \\ K^{21(e)} & K^{22(e)} \end{bmatrix} \begin{Bmatrix} u^{(e)} \\ u^{(e)} \end{Bmatrix} = \begin{Bmatrix} F^{1(e)} \\ F^{2(e)} \end{Bmatrix}$$

and rearrange this system to get

$$[K^{(e)}]\{\triangle^{(e)}\} = \{F^{(e)}\},$$

where

$$\{\triangle^{(e)}\} = [u_1^{(e)}, v_1^{(e)}, u_2^{(e)}, v_2^{(e)}, ..., u_n^{(e)}, v_n^{(e)}]^T,$$

$$\{F^{(e)}\} = [F_1^{1(e)}, F_1^{2(e)}, F_2^{1(e)}, F_2^{2(e)}, ..., F_n^{1(e)}, F_n^{2(e)}]^T.$$

The $[\ ]^T$ implies the transpose of the matrix $[\ ]$.

3. RESULTS AND DISCUSSION

3.1. **1kW-class HAWT rotor blade model designed by BEMT.** The optimum design parameters of 1kW-class HAWT rotor blade are shown in Table 1 and the blade element momentum theory developed in Sect. 2.1 is applied to obtain the boundary conditions for elastic characteristics. Fig. 1 presents the schematic view of 1kW-class HAWT rotor blade model. Airfoil profile of NACA 63(2)-415 is applied to the total radial length of the rotor blade. The composite rotor blade is of the longitudinal length of the blade $R = 1250mm$ and the lateral length $Y = 310mm$.

In Fig. 2(a), the relative flow angle, and axial and angular induction factors of the rotor blade are displayed through graphs. The relative flow angle decreases exponentially with the increase of normalized radius (NR). The angular induction factor decreases exponentially until the value of NR is 0.3 and the rate of decrease is proportional to a linear function after NR 0.3. The induction factor increases around the interval $0.3 < NR < 0.85$, while decrease rapidly after NR 0.85. Fig. 2(b) presents the stresses, axial force, tangential force, and torque, occurring on

TABLE 1. Value of parameters.

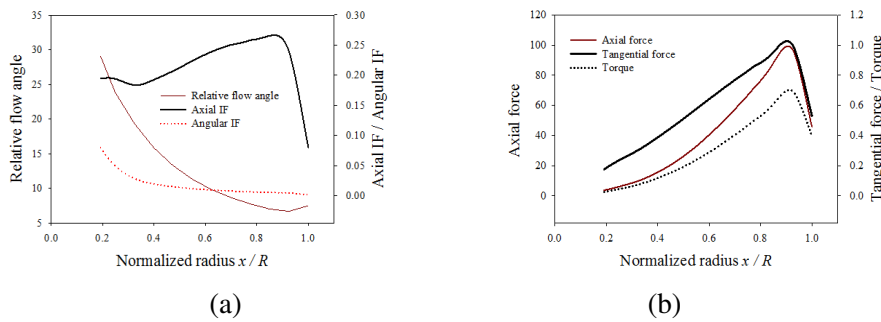| Parameter	value
Number of blade	3
Blade rotational speed	$500/min$
Wake rational speed	$3m/s\ (11km/h)$
Absolute velocity	$9m/s\ (32km/h)$
Density	$1.255kg/m^3\ (1kg/m^3 = 0.001g/cm^3)$
Tip speed ratio	7

(a)   (b)

FIGURE 2. Design parameters of 1kW-class HAWT rotor blade model calculated by BEMT : (a) axial and angular induction factor, relative flow angle, (b) axial and tangential forces, torque.

the rotor blade of wind turbine. The axial force increases exponentially until NR 0.85 with the increase of NR and decreases rapidly after NR 0.85. But, Fig. 2(b) exhibits a linear growth in the variation of tangential force until NR 0.85. Similar behavior is appeared in the variation of torque. Fig. 3 shows the performance curve by power coefficient (C_p) according to the tip speed ratio (λ), based on CFD analysis on the 1kW-class HAWT rotor blade designed [20]. The power coefficient is defined as

$$C_p = \frac{P}{\frac{1}{2}\rho A V_\infty^3}.$$

When λ is 7, C_p presents the maximum value of 0.48. As the inlet wind velocity is $9.3m/s$ which is corresponding to $\lambda=7$, and about 1.2kW output power is generated on the condition of the standard atmospheric pressure air density, it is considered that the design method of the rotor blade by BEMT in this study is reliable enough.

3.2. **Elastic characteristics of the composite rotor blade model.** For the elastic characteristics of a composite rotor blade a finite element method is developed to obtain the numerical
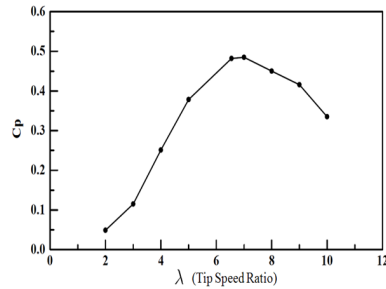
FIGURE 3. Power coefficient curve by BEMT.

TABLE 2. Mechanical properties used for analyzing elastic characteristics.

Material / Property	E_1(GPa)	E_2(GPa)	G_{12}(GPa)	ν_{12}	ν_{21}
C520	48.2	11.7	6.48	0.3	0.3
3/4 Mat	7.58	7.58	6.48	0.3	0.3
Gel Coat	3.44	3.44	1.32	0.3	0.3

solutions using the boundary conditions displayed in Fig. 2(b). The discritized rotor blade is sketched in Fig. 1(c) and the process in Sect. 2.3 is applied to obtain numerical solutions. The mechanical properties for elastic characteristics are shown in Table 2.

Figure 4 indicates the displacements of the laminate piling up with five ply in sequence [0/0/0/0/0]. The middle ply has 6.0 mm thickness and the other plies are 1.0 mm thickness. The normalized longitudinal and lateral displacement components u_x/R and u_y/Y are presented to normalized position x/R and y/Y, respectively, in Fig. 4. The representative normalized positions are x/R=0.248, x/R=0.546, and x/R=843. In the longitudinal displacement, the lower part of the blade is under the action of compression and the upper part of the blade is extended at x/R=0.248, while the blade, at x/R=0.546, displays positive extension at the lower part and the upper part is compressed with larger magnitude (see Fig. 4(a)). Near the tip of the blade, x/R=843, most area of the blade experiences positive extension. As shown in Fig. 4(b), only positive lateral displacement appears and the magnitude of the lateral displacement increases as the normalized x/R increases. The movement is rhythmical occurring sinuous-type fluctuation, and larger lateral displacement proceeds at the boundary of the lower part, which demonstrates that the mathematical approach is reliable and reasonable.

For the representative normalized positions x/R=0.248, and x/R=0.546, the stresses are exhibited in Fig. 5 of the laminate piling up with five-ply in sequence [0/0/0/0/0]. At x/R=0.248, the lower part of the blade is under the loading of compressive longitudinal stress except near the boundary and the compressive stress converts into the tensile after y/Y=0.456 (see Fig. 5(a)), which implies that the upper of the blade is exposed to the failure mechanism and more fragile. The maximum magnitude of the compressive longitudinal stress occurs around
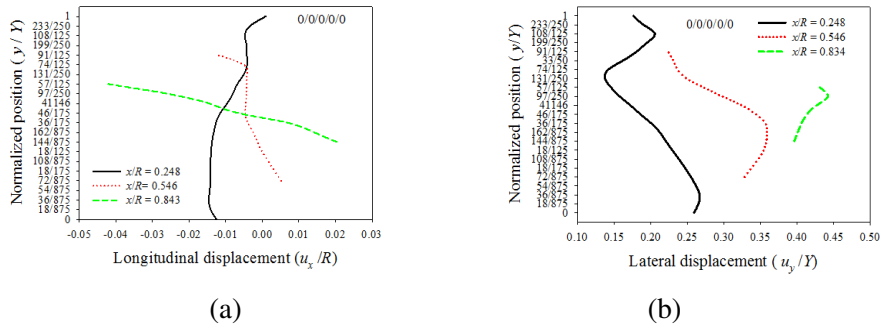
FIGURE 4. Displacements of the laminate by normalized positions : (a) longitudinal, (b) lateral displacement.
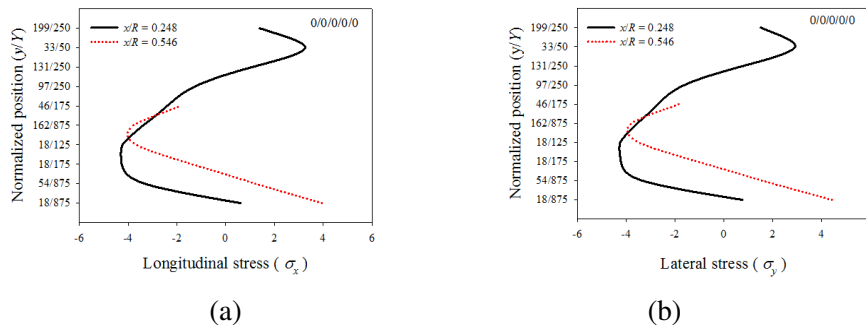

FIGURE 5. Stresses of the laminate by normalized positions : (a) longitudinal stress, (b) lateral stress.

y/Y=0.115 and the tensile longitudinal stress around y/Y=0.66. Similar behavior develops in the lateral stress, as shown in Fig. 5(b).

The effects of the piling sequence of five-ply are analyzed through Figs. 6-7. Four different piling styles: [0/0/0/0/0], [0/(π/2)/0/(π/2)/0], [0/0/(π/2)/0/0], and [0/(π/2)/(π/2)/(π/2)/0] are chosen to investigate the elastic characteristics of the composite blade at the normalized position x/R=0.546. The blade with piling sequence [0/0/0/0/0] and [0/(π/2)/0/(π/2)/0] is compressed in the longitudinal direction over the normalized interval $y/Y < 0.67$ and extended to the positive longitudinal direction over the normalized interval $y/Y > 0.67$ (see Fig. 6(a)). In the piling sequence [0/0/(π/2)/0/0] and [0/(π/2)/(π/2)/(π/2)/0] the longitudinal displacement develops to the positive direction over the interval $y/Y < 0.144$, but, the blade is compressed over the interval $y/Y > 0.144$. Fig. 6(b) displays the lateral displacement at the normalized position x/R=0.546. The lateral displacement is compressed in the piling sequence [0/0/0/0/0] and [0/(π/2)/0/(π/2)/0], whereas the blade is extended to the positive direction in the piling

sequence $[0/0/(\pi/2)/0/0]$ and $[0/(\pi/2)/(\pi/2)/(\pi/2)/0]$. The movements of the blade are al-most identical in the piling sequence $[0/0/0/0/0]$ and $[0/(\pi/2)/0/(\pi/2)/0]$, and, $[0/0/(\pi/2)/0/0]$ and $[0/(\pi/2)/(\pi/2)/(\pi/2)/0]$, respectively, expressing that the piling angle of the middle layer yields crucial influence on the elastic characteristics.
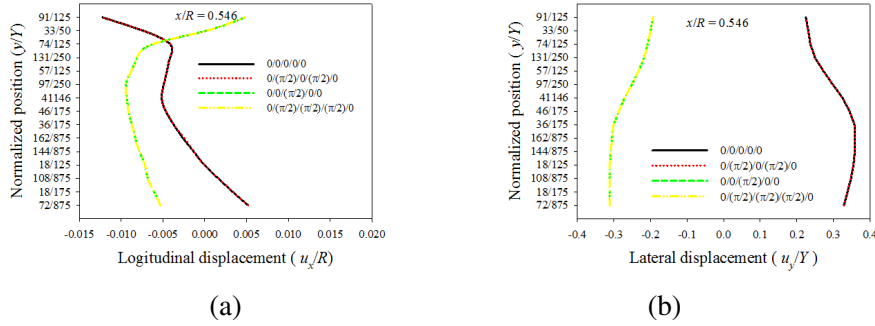

FIGURE 6. Displacements of laminate by piling sequence : (a) longitudinal, (b) lateral.

The stress distribution profiles are expressed in Fig. 7 at the normalized position x/R=0.546. In the piling sequence $[0/0/0/0/0]$ and $[0/(\pi/2)/0/(\pi/2)/0]$ longitudinal tensile stress develops over the interval $y/Y < 0.0823$ and the longitudinal stress converts into compressive over the other interval $y/Y > 0.0823$ (see Fig. 7(a)). But, the blade with the piling sequence $[0/0/(\pi/2)/0/0]$ and $[0/(\pi/2)/(\pi/2)/(\pi/2)/0]$ is under the loading of tensile stress except the nearby of lower boundary. As shown in Fig. 7(b) similar tendency develops in the lateral stress distribution profiles except for the magnitude of tensile stress in the piling sequence $[0/0/(\pi/2)/0/0]$ and $[0/(\pi/2)/(\pi/2)/(\pi/2)/0]$. The shear stress distribution profiles are dis-played in Fig. 7(c). The blade with the piling sequence $[0/0/0/0/0]$ and $[0/(\pi/2)/0/(\pi/2)/0]$ is pressured with compressive shear stress, while tensile stress is appeared over the interval $y/Y > 0.144$ in the piling sequence $[0/0/(\pi/2)/0/0]$ and $[0/(\pi/2)/(\pi/2)/(\pi/2)/0]$. The results demonstrate that composite blades with the piling sequence $[0/0/0/0/0]$ and $[0/(\pi/2)/0/(\pi/2)/0]$ express more durable.
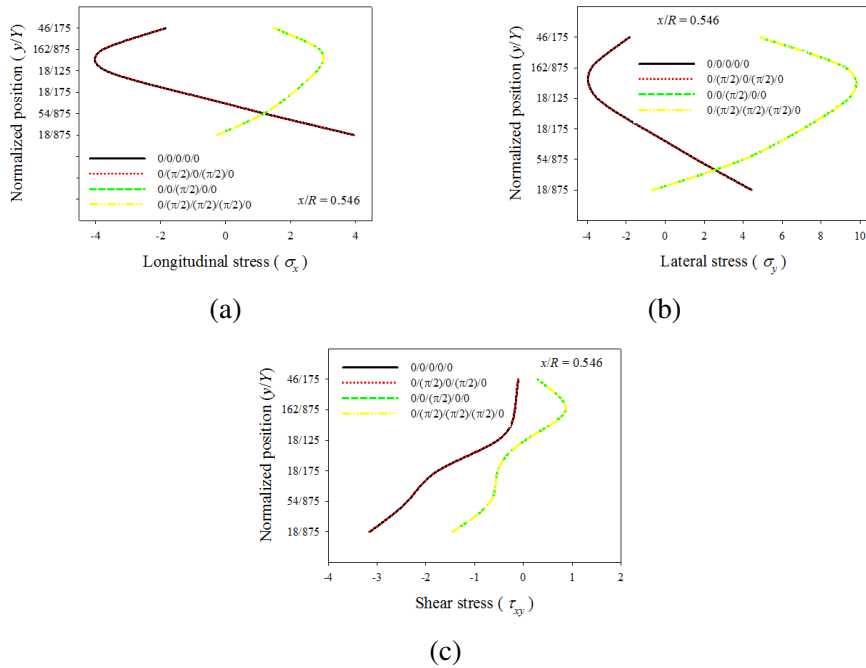
FIGURE 7. Stresses of laminate by piling sequence : (a) longitudinal, (b) lateral, (c) shear.

4. CONCLUSIONS

The elastic characteristics of composite blades subjecting wind loading have been investigated through mathematical approach. The relative flow angle, axial and angular induction factors, and the stresses on the boundary are sensitive to the shape of rotor blade. A sinuous-type fluctuation appears in the movement of the rotor blade, and larger lateral displacement proceeds at the boundary of the lower part demonstrating reasonable mathematical. The conversion in stress distribution profiles is a cause of failure mechanisms during the life time. The piling sequence is an important factor to determine elastic characteristics in composite rotor blades. Especially, the piling angle of the middle layer exerts a crucial influence on the rotor blade behavior, and the same piling angle at the middle layer expresses almost identical elastic movement. The results will be helpful in designing a composite rotor blade.

ACKNOWLEDGMENTS

References

[1]]D.A. Spera, *Wind turbine technology*, New York: ASME Press; 1994.

[2] M. M. Shokrieh, and R. Rafiee, *Simulation of fatigue failure in a full composite wind turbine blade*, Composite Structures **74** (2006) 332-342.

[3] Y.-C. TSENG, and C.-Y. KUO, *Engineering and Construction Torsional Responses of Glass- Fiber/Epoxy Composite Blade Shaft for A small Wind Turbine*, Procedia Engineering **14** (2011) 1996-2002.

[4] L.C.T. Overgaard , E. Lund, and P.P. Camanho, *A methodology for the structural analysis of composite wind turbine blades under geometric and material induced instabilities*, Computers and Structures **88** (2010) 1092-1109.

[5] C. W. Kensche , *Fatigue of composites for wind turbines*, International Journal of Fatigue **28** (2006) 1363-1374.

[6] H. Ghasemnejad, L. Occhineri, and D.T. Swift-Hook, *Post-buckling failure in multi delaminated composite wind turbine blade materials*, Materials and Design **32** (2011) 5106-5112.

[7] M.C. Aceves, A.A. Skordos, and M.P.F. Sutcliffe, *Design selection methodology for composite structures*, Mater Design, **29** (2008), 418-4261.

[8] C. M. Aceves, M.P.F. Sutcliffe, M.F. Ashby, A.A. Skordos, and C. Rodriguez Roman, *Design methodology for composite structures: A small low air-speed wind turbine blade case study*, Materials and Design **36** (2012) 296-305.

[9] E. Lindaard and E. Lund, *Nonlinear buckling optimization of composite structures*, Computer Methods in Applied Mechanics and Engineering **199** (2010) 2319-2330.

[10] X. Chen, J. Tang, and K. Yang, *Modeling multiple failures of composite box beams used in wind turbine blades*, Composite Structures **217** (2019) 130-142.

[11] H.G. Lee and J. Lee, *Damping mechanism model for fatigue testing of a full-scale composite wind turbine blade, Part 1: Modeling*, Composite Structures **202** (2018) 1216-1228.

[12] V. Giavotto, M. Borri, P. Mantegazza, G. Ghiringhelli, V. Carmaschi, G. Maffioli, and F. Mussi, *Anisotropic beam theory and applications*, Comput. Struct. **16** (1983) 490-413.

[13] J. Blasques, R. Bitsche, V. Fedorov, and B. Lazarov, *Accuracy of an efficient framework for structural analysis of wind turbine blades*, Wind Energy **19** (2015) 1603-1621.

[14] W. Yu, D.H. Hodges, and J.C. Ho, *Variational asymptotic beam sectional analysis-an updated version*, Int. J. Eng. Sci. **59** (2012) 40-64.

[15] I. Fleming and D.J. Luscher, *A model for the structural dynamic response of the CX-100 wind turbine blade*, Wind Energy **17** (2013) 877-900.

[16] Q. Wang, M.A. Sprague, J. Jonkman, N. Johnson, and B. Jonkman, *BeamDyn:a high-fidelity wind turbine blade solver in the FAST modular framework*, Wind Energy (2017)

[17] X. Zhou, K. Huang, and Z. Li, *Geometrically nonlinear beam analysis of composite wind turbine blades based on quadrature element method*, International Journal of Non-Linear Mechanics **104** (2018) 87-99.

[18] T. Burton, D. Sharpe, N. Jenkins, and E. Bossanyl, *Wind Energy Handbook*, 2001, John Wiley & Sons, Ltd.

[19] R.M. Jones, *Mechanics of Composite Materials*, 2nd edition, 1999, Taylor & Francis.

[20] J-Y. Lee, N-J, Choi, J-W Lee, H-Y Yoon and Y-D Choi, *Shape Design and CFD Analysis on a 1kW-class Horizontal Axis Wind Turbine Blade for Hybrid Power Generation System*, Proc. Of The 11th Asian International Conference on Fluid Machinery and The 3rd Fluid Power Technology Exibition (2011) Paper number 120.